Satellite data assimilation to improve forecasts of volcanic ash concentrations: a case study on the 2010 Eyjafjallajökull volcanic ash plume

Guangliang Fu[1], Hai Xiang Lin[1], Arnold Heemink[1], Arjo Segers[2], Fred Prata[3], and Sha Lu[1]

[1]Delft University of Technology, Delft Institute of Applied Mathematics, Mekelweg 4, 2628 CD Delft, The Netherlands.
[2]TNO, Department of Climate, Air and Sustainability, P.O. Box 80015, 3508 TA Utrecht, The Netherlands.
[3]Nicarnica Aviation AS, Gunnar Randers vei 24, NO-2007 Kjeller, Norway.

Correspondence to: Guangliang Fu (G.Fu@tudelft.nl)

Abstract. Data assimilation is a powerful tool that requires available observations to improve model forecast accuracy. Infrared satellite measurements of volcanic ash mass loadings are often used as input observations for the assimilation scheme. However, these satellite-retrieved data are often two-dimensional (2D), and cannot easily be combined with a three-dimensional (3D) volcanic ash model to improve the volcanic ash state. By integrating available data including ash mass loadings, cloud top heights and thickness information, we propose a satellite observational operator (SOO) that translates satellite-retrieved 2D volcanic ash mass loadings to 3D concentrations at the top layer of the ash cloud. Ensemble-based data assimilation is used to assimilate the extracted measurements of ash concentrations. The results show that satellite data assimilation can force the volcanic ash state to match the satellite observations, and that it improves the forecast of the ash state. Comparison with highly accurate regional aircraft in situ measurements shows that the effective duration of the improved regional volcanic ash forecasts is about a half day.

1 Introduction

It has been known for many years that volcanic ash is dangerous to commercial jet aircraft (Casadevall, 1994). Little is known about the exact level of ash concentrations that becomes dangerous to the jet turbine, and the current recommendation states that the highest concentration an aircraft can endure is 4.0 mg m^{-3} (EASA, 2015). Until carefully designed engine performance tests are conducted in realistic volcanic ash cloud conditions, a cautious approach to advising commercial jet operations in airspace is recommended. As a consequence, the eruption of the Eyjafjallajökull volcano in Iceland from 14 April to 25 May 2010, caused an unprecedented closure of the European and North Atlantic airspace resulting in a huge global economic loss of up to 5 billion US dollars (Oxford-Economics, 2010). Due to the major impacts on the aviation community, a lot of research has been initiated on how to efficiently reduce these aviation impacts, starting with improving the accuracy of volcanic ash forecasts after eruption onset (Eliasson et al., 2011; Schumann et al., 2011).

For forecasting volcanic ash plumes, many Volcanic Ash Transport and Dispersion Models (VATDM) are worldwide available, e.g., PUFF (Searcy et al., 1998), HYSPLIT (Draxler and Hess, 1998), ATHAM (Oberhuber et al., 1998), NAME (Jones

et al., 2007) and LOTOS-EUROS (Fu et al., 2015). Literatures have reported in-depth comparisons between volcanic ash real-time advisories and volcanic ash transport models (Witham et al., 2007; Webley et al., 2012). The meteorological wind fields and estimates of eruption source parameters (ESPs) such as plume height (PH), mass eruption rate (MER), particle size distribution (PSD) and vertical mass distribution (VMD) are necessary as inputs to the VATDM (Mastin et al., 2009). A VATDM uses physical parameterizations of particle sources and removal processes (including sedimentation and deposition) that affect the concentrations in a dispersing volcanic plume. Without accurate knowledge of the ash removal rate in atmospheres and the temporal variation of MER at the volcano, it is impossible to provide quantitatively accurate concentration forecasts for the ash plume arriving in an airspace over a long distance (Prata and Prata, 2012; Fu et al., 2016).

For the purpose of improving the forecast accuracy of volcanic ash concentrations, efficient technologies must be employed to compensate the VATDM's inaccuracies. Data assimilation, which refers to the (quasi-) continuous use of the direct measurements to create accurate initial conditions for model runs, is one of the most commonly used approaches for real-time forecasting problems (Evensen, 2003; Bocquet et al., 2015; Fu et al., 2015). In each assimilation step, a forecast from the previous model simulation is used as a first guess, then available observations are used to modify this forecast in better agreement with these observations. An important aspect of the assimilation approach is that it reduces the dependency on accurate knowledge of the ESPs– which are generally unknown at the time of an eruption. This is an effective approach where valid real-time volcanic ash measurements are required to guarantee the forecast accuracy (Fu et al., 2015). Fortunately, during volcanic ash transport, different types of scientific measurement campaigns were performed to collect information of the ash plume. The measurements contained e.g., ground-based lidar and ceilometer measurements (Pappalardo et al., 2010; Wiegner et al., 2012), satellite observations (Stohl et al., 2011; Prata and Prata, 2012; Lu et al., 2016a), aircraft-based measurements (Schumann et al., 2011; Weber et al., 2012; Schäfer et al., 2011), ground-based in situ measurements (Emeis et al., 2011), balloon measurements (Flentje et al., 2010) and ground-based remote sensing Sun photometer observations (Ansmann et al., 2010). However, it should be noted that such measurements usually are not available globally and for remote volcanoes it is usually hard to perform measurement campaigns, especially as consequence of sudden eruptions.

Satellite measurements are of special interest, because the detection domain is large and the output data is long-time continuous. For example, the Spin Enhanced Visible and Infrared Imager (SEVIRI), on board the Meteosat Second Generation (MSG) platform provides a large view coverage of the atmosphere and earth's surface (Schmetz et al., 2002). There are 3712 $\times$ 3712 pixels covering the full-disk. Images can be acquired for the whole disk every 15 minutes. These satellite data have been used for many years to retrieve ash mass loadings in a dispersing volcanic plume (Prata and Prata, 2012). Nowadays, ash mass loadings (Prata and Prata, 2012), the effective particle size (Kylling et al., 2015) as well as the ash cloud top height (Francis et al., 2012), are available in near real-time as satellite products during volcanic plume transport. The availability of satellite-based data provides us with an opportunity to employ data assimilation with a VATDM to continuously correct the volcanic ash state, and then improve the forecast accuracy of volcanic ash concentrations.

There still exist difficulties on how to efficiently use volcanic ash mass loadings, because a VATDM is in most cases a 3D model, while the satellite-retrieved ash mass loadings are 2D data. One 2D mass loading can be considered as an integral of ash concentrations along a retrieval path (the path can be a line or a curve which depends on a specified retrieval algorithm) (Prata

and Prata, 2012). Thus, the 2D measurements are not directly suited in a 3D data assimilation system. Since satellites provides 2D ash mass loadings and the model has 3D concentrations, an observational operator is needed by the data assimilation algorithm, and must be derived to make both types of information directly comparable. For this purpose, vertical information of the ash cloud, such as the ash cloud top height (de Laat and van der A, 2012), the cloud thickness and the corresponding uncertainties, should be included. Cloud-Aerosol Lidar with Orthogonal Polarization (CALIOP) (Winker et al., 2012) lidar measurements can provide detailed vertical information on plumes, but the measurements are spatially sparse and have low temporal resolution (polar-orbit) and the data processing and delivery is not designed for near real-time applications. Thus CALIOP data is not suitable to provide the near real-time thickness information for the overall volcanic ash plume.

For the vertical thickness information of volcanic ash clouds, Schumann et al. (2011) investigated on the 2010 Eyjafjallajökull eruption using airborne data that the volcanic ash clouds spread over large parts of Central Europe, mostly from hundreds to 3 km depth. This is consistent with the results of (Marenco et al., 2011) who observed layer depths between 0.5 and 3.0 km. Dacre et al. (2015) also examined the ground-based lidar data for the Eyjafjallajökull eruption and found a mean layer depth of 1.2 ± 0.9 km and compared this with model based estimates of 1.1 ± 0.8 km. Prata and Prata (2012) found variable thicknesses ranging from 0.2 up to 3 km. Recently, Clarisse and Prata (2016) reported 16 cases using ground-based lidar measurements during the Eyjafjallajökull eruption and found 3 cases where the cloud thickness was less than 500 m. Cloud thicknesses for Kasatacho (1.01 ± 0.43 km), Sarychev Peak (1.37 ± 0.42 km) and Puyehue-Cordon Caulle (1.80 ± 0.58 km) (private communication) all exceed 1 km, but Prata et al. (2015) reported lower cloud thickness with 80% of cases for the 2006 Chaiten eruption less than 400 m. The vast majority of data suggest thickness in the range 0.5–3 km, but it is entirely possible that thinner clouds (<400 m) do exist. Such clouds must have higher concentrations to be detectable by current infrared satellite techniques (Prata and Prata, 2012; Pavolonis, 2010)) that suggest a lower sensitivity in mass loading of 0.2 g m^{-2}. Thin ash clouds, by their nature are of less concern to aviation because such clouds would be traversed rapidly avoiding the possibility of particle build-up that might lead to engine failure. From a modeling perspective lack of vertical resolution in model wind data makes it not useful to make the cloud depth any less than 500 m.

Based on these investigations, it is not realistic to use a deterministic value to represent the overall ash cloud thickness, but we can reasonably assume that the thickness has a range of 0.5–3.0 km at the corresponding horizontal location of the SEVIRI retrieved measurements. Although this thickness information is not deterministic, its uncertainty spread is suitable in an observational operator for satellite data assimilation. Note that we are only considering the distal plume, at least the part >100 km's from source, which is because close to the emission source the layering of volcanic ash did not necessarily take place.

In this paper we focus on the case study of the Eyjafjallajökull volcanic ash plume in May 2010. In order to integrate data and information about volcanic ash clouds, the first goal in this study is to develop a satellite observational operator to translate satellite-retrieved 2D ash mass loadings to 3D concentrations at the top layer of the ash cloud. Secondly, using the extracted in situ measurements, we investigate whether ensemble-based data assimilation can significantly improve the volcanic ash state. Finally, the effective duration of the improved volcanic ash forecasts after satellite data assimilation is quantified.

2 Available data for data assimilation

In this study, geostationary SEVIRI observations for the 2010 Eyjafjallajökull volcanic eruption plume (Prata and Prata, 2012) are used as the study case to design a suitable satellite observational operator (SOO) for data assimilation. SEVIRI is a 12-channel spin-stabilized imaging radiometer. Measurements are made with a spatial resolution from 3 km $\times$ 3 km at the sub-satellite point to 10 km $\times$ 10 km at the edges of the scan. A region covering 30° W to 15° E and 45° N to 70° N is selected here for analysis which includes the geographic area affected by the Eyjafjallajökull volcanic ash (see Fig. 1).

The main retrieval products from SEVIRI are ash mass loadings (Prata and Prata, 2012; Kylling et al., 2015) (see Fig. 1**a**, value at 0 means no data) where 03:15 UTC 16 May 2010 is chosen for the illustration, without loss of generality. The mass loading at each 2D pixel gives information on the ash cloud from the top view (Prata and Prata, 2012), which can be taken as an integration of ash concentrations along the retrieval path. Besides ash mass loadings, other products including the ash cloud top height (Fig. 1**b**), and the error of ash mass loadings (Fig. 1**c**) are also available in a near real-time sense (Francis et al., 2012; Prata and Prata, 2012). As a parameter used in SEVIRI retrievals, the data of ash cloud top height is adopted with the SEVIRI-KNMI product of ash height, which has been evaluated with a reasonable accuracy, as reported by de Laat and van der A (2012). The error of ash mass loadings indicates the uncertainty and accuracy of the retrieved mass loadings.

All the data shown in Fig. 1 are acquired from the European Space Agency (ESA) funded project – Volcanic Ash Strategic Initiative Team (VAST). The VAST retrieval utilizes two techniques: 1) A rudimentary cloud detection scheme implemented in the Eumetsat operational scheme caled "VOLE" (http://navigator.eumetsat.int/discovery/Start/DirectSearch/DetailResult.do?f%28r0%29=EO:EUM:DAT:MSG:VOLE), and 2) A more complex scheme called CID (Cloud Identification). This scheme is described in an Algorithm Theoretical Basis Document (ATBD) (unpublished but available here: (http://vast.nilu.no/satellite-observations/)). We have used retrievals from the CID scheme. In this study, additional processing on the retrieved data is needed to translate the data from the original SEVIRI resolution to the VATDM resolution.

Limited validation has shown that the satellite ash retrievals are sufficiently accurate for use with dispersion models to correct ash concentration forecasts (Prata and Prata, 2012; Kylling et al., 2015). However, the correction cannot be directly and automatically implemented by data assimilation due to the insufficient vertical resolution in satellite data (Bocquet et al., 2015).

3 Satellite observational operator (SOO)

3.1 Derivation

The derivation of the satellite observational operator (SOO) is shown in Fig. 2. The retrieved values by SEVIRI for the ash mass loadings (ML) can be taken as an integration of ash concentrations along the retrieval path. In principle, the satellite retrieval path could be complicated but generally it is assumed to be a straight line (along the line-of-sight, ignoring refraction) from the measuring apparatus. The angle between the local zenith and the line of sight to the satellite is called Viewing Zenith Angle (VZA). The VZA for each pixel is computed according to the satellite VZA algorithms (Gieske et al., 2005) by using

general parameters (such as longitude, latitude of each pixel). With the cosine of this angle and the retrieved ash mass loadings (ML), the mass loadings in the vertical direction ($\mathrm{ML_{vert}}$) can be calculated by Eq. (1),

$$\mathrm{ML_{vert}} = \mathrm{ML} \times \cos(\mathrm{VZA}). \tag{1}$$

To extract ash concentrations from SEVIRI retrievals, $\mathrm{ML_{vert}}$ only is not sufficient and knowledge about the vertical distribution of ash cloud must be included. The cloud vertical profile can be described with the height of the top and the thickness of the cloud. As introduced in Section 2, the cloud top height ($\mathrm{H_{top}}$) is available from satellite remote sensing and the thickness of the plume is investigated ($\mathrm{T_{low}}$ to $\mathrm{T_{high}}$, i.e., 0.5 to 3 km). Fig. 2 illustrates how the 3D ash concentrations are extracted from the obtained mass loadings in the vertical direction ($\mathrm{ML_{vert}}$). The blue layer in Fig. 2 is determined by the lowest possible thickness ($\mathrm{T_{low}}$) and the extraction layer used in this study only refers to the blue layer.

When the top height and the thickness range of ash cloud are known, the ash concentration (C) in the extraction layer can be calculated by using the ash mass loadings ($\mathrm{ML_{vert}}$) at the corresponding horizontal location. The details are formulated as follows. First we define

$$N_s = \left\lceil \frac{\mathrm{T_{high}} - \mathrm{T_{low}}}{\mathrm{T}} \right\rceil \quad , \tag{2}$$

$$\mathrm{T}_i = \mathrm{T_{low}} + (i-1) \times \mathrm{T}, \quad \mathrm{C}_i = \frac{\mathrm{ML_{vert}}}{\mathrm{T}_i}, \qquad i = 1, 2, \cdots, N_s \quad , \tag{3}$$

where T is a step length and N_s is the number of the possible thickness. $\mathrm{T_{low}}$ represents the blue layer (see Fig. 2) with the fixed thickness of 0.5 km and $\mathrm{T_{high}} - \mathrm{T_{low}}$ represents the yellow layer with the fixed thickness of 2.5 km. T is chosen at a small value compared to $\mathrm{T_{low}}$, which guarantees N_s is not too small (e.g., less than 2) to sample sufficient number of thickness $\mathrm{T}_1, \mathrm{T}_2, \cdots, \mathrm{T}_{N_s}$ with equal probability. (e.g., T is chosen as 0.05 km in this case study, thus N_s is calculated as 50.)

Corresponding to the sampled thickness, the ash concentration can be calculated also as a sample from C_1 to C_{N_s}, as shown in Eq. (3). Therefore, the mean ($\mathrm{C_{mean}}$) and the standard deviation ($\mathrm{C_{std}}$) of the sampled ash concentrations can be calculated by Eq. (4) and (5),

$$\mathrm{C_{mean}} = \frac{1}{N_s}(\mathrm{C}_1 + \mathrm{C}_2 + \cdots + \mathrm{C}_{N_s}) \quad , \tag{4}$$

$$\mathrm{C_{std}} = \sqrt{\frac{1}{N_s - 1}[(\mathrm{C}_1 - \mathrm{C_{mean}})^2 + (\mathrm{C}_2 - \mathrm{C_{mean}})^2 + \cdots + (\mathrm{C}_{N_s} - \mathrm{C_{mean}})^2]} \quad . \tag{5}$$

$\mathrm{C_{mean}}$ is therefore used in this study as the extracted concentration C between the heights [$\mathrm{H_{top}}$ - $\mathrm{T_{low}}$] and $\mathrm{H_{top}}$ (i.e., the blue layer in Fig. 2). How much of the mass is distributed to the blue layer ($\mathrm{ML_{blue}}$) can be calculated by Eq. (6),

$$\mathrm{ML_{blue}} = \mathrm{C_{mean}} \times \mathrm{T_{low}}. \tag{6}$$

Note that, below the height [$\mathrm{H_{top}}$ - $\mathrm{T_{low}}$] (the yellow layer shown in Fig. 2), ash concentrations should not be extracted, because the concentrations there can be zero. For example, when $\mathrm{H_{top}}$ equals to 8.0 km and the cloud's thickness is 1.0 km, thus ash concentrations between 7.5 km and 8.0 km can be obtained from Eq. (4). However, the ash concentrations at 5.0 km cannot be extracted because actually there is no concentration at that height. Another note is that Eq. (5) is calculated based on

the most commonly used assumption of Gaussian distribution in error analysis. Gaussian often occurs in nature, and by lack of other information this is therefore a suitable first choice.

3.2 Extraction error

Fig. 2 and Eq. (2) to (5) describe the details of the SOO. The operator transforms the 2D ash mass loadings (ML) to 3D ash concentrations (C, here C=$\mathrm{C_{mean}}$). Fig. 3**a** shows the extracted ash concentrations (C) at the cloud top layer. It can be seen that the extracted ash concentrations in the ash plume are between 0.1 and 0.9 mg $\mathrm{m^{-3}}$.

Now we quantify the extraction error $\mathrm{C_{error}}$ (i.e., error in the extracted concentrations), which is important for a data assimilation system. The extraction error is not equivalent to $\mathrm{C_{std}}$, but depends on both the retrieval error $\mathrm{ML_{error}}$ (error in mass loadings, as shown in Fig. 1**c**) and $\mathrm{C_{std}}$. The dependence is described by Eq. (7) in terms of uncertainty,

$$\mathrm{U_C} = 1 - (1 - \frac{\mathrm{ML_{error}}}{\mathrm{ML}})(1 - \frac{\mathrm{C_{std}}}{\mathrm{C}}) \quad , \tag{7}$$

where the uncertainty ($\mathrm{U_C}$) of the extracted concentrations is calculated based on the derivation uncertainty ($\frac{\mathrm{C_{std}}}{\mathrm{C}}$, normalized standard deviation) and the retrival uncertainty ($\frac{\mathrm{ML_{error}}}{\mathrm{ML}}$). Eq. (7) is defined according to the fact that the extraction is performed on the uncertain ash mass loadings, indicating the conditional probability relation. Now $\mathrm{U_C}$ is quantified, the error ($\mathrm{C_{error}}$) in the extracted concentrations can be easily obtained by Eq. (8),

$$\mathrm{C_{error}} = \mathrm{C} \times \mathrm{U_C} \quad . \tag{8}$$

Fig. 3**b** illustrates the extraction error $\mathrm{C_{error}}$, which together with C describes the 3D measurements (mean, error) for ensemble-based data assimilation.

The outcome of SOO can be considered as preprocessing to the satellite data assimilation system. The extracted data only represents the data at the cloud top height, which can be taken as the data within the 0.5 km layer thickness. The other layer thickness is also of high importance, which is used for the derivation of uncertainties.

4 Assimilation of satellite-extracted ash concentrations

4.1 Satellite data assimilation system

An ensemble-based data assimilation technique is used in this study to assimilate the SEVIRI-based ash concentrations extracted by SOO. After the ensemble Kalman filter was proposed by Evensen (1994), many other algorithms were developed such as the reduced rank square root filter (Verlaan and Heemink, 1997), the ensemble Kalman smoother (Evensen and van Leeuwen, 2000), ensemble square root filter (Evensen, 2004). Ensemble-based data assimilation allows a very general statistical description of errors and is suitable for estimation of concentrations (Evensen, 2003). Based on the ensemble formulation, the dynamical model is not restricted to linearity and the implementation of the algorithm is very simple (Bocquet et al., 2015). The ensemble square root filter (EnSR, see Appendix A), in most applications a more efficient method (Evensen, 2004) than the

ensemble Kalman filter, is employed in this study to perform the ensemble-based data assimilation. Note that the observational operator ($\mathbf{H}$, see Appendix A) used in EnSR is different from SOO. SOO is an operator designed as a preprocessing procedure before data assimilation, which doesn't depend on the model space and aims to transfer 2D satellite data into 3D measurements for later usage in EnSR. While, $\mathbf{H}$ is an intrinsic operator in the EnSR algorithm as specified in Appendix A.

To simulate volcanic ash transport, the LOTOS-EUROS model (Schaap et al., 2008) is used in this study. The configurations and evaluations of the LOTOS-EUROS as a proper volcanic ash transport model was reported by Fu et al. (2015). The model run starts at 00:00 UTC 15 May 2010 with an initial ash load obtained from previous LOTOS-EUROS model run. As the model state changes with time in the numerical simulation (the time step of the model run is 15 minutes used by Fu et al. (2015)), the model result from the previous time step is taken as the initial state for the next time step. When the model run arrives at 01:00 UTC 16 May, the volcanic ash state gets continuously modified by the data assimilation process until 00:00 UTC 18 May, by combining the extracted measurements of ash concentrations. The specification of uncertainties is essential for a successful data assimilation. Here we use uncertainties in plume height (PH). PH is set to be the radar detection data from Icelandic Meteorological Office (IMO) and its uncertainty is estimated to be 20 % (Bonadonna and Costa, 2013). The stochastic plume height (PH) is assumed to be temporally correlated with exponential decay and the correlation parameter τ is set to be 1 hour (Fu et al., 2015). Thus, the PH noise (N_{ph}) at two times (t_1 and t_2) has the relation (Evensen, 2004) of $\mathbb{E}[N_{ph}(t_1) \cdot N_{ph}(t_2)] = e^{\frac{-|t_1-t_2|}{\tau}}$, where $\mathbb{E}$ represents the mathematical expectation.

4.2 Total measurement error

To assimilate measurements in a simulation model, the total measurement error must be first estimated, which not only contains the extraction error (Section 3.2), but also includes an estimate of the model representation error (Fu et al., 2015). The model representation error is the discrepancy between the measurement location and where the model can represent the measurement. Concentration values are defined on discrete grids with a finite resolution at discrete time steps. The grid resolution of the model used in the study is 0.25° longitude × 0.125° latitude × 1 km altitude, while the SEVIRI pixel size here is 0.1° longitude × 0.1° latitude. After a careful check on the SEVIRI measurements, a measurement location does not coincide with the grid center point where the concentration value is defined. In this study, a preprocessing procedure before data assimilation is employed to average all measurements in a model grid to generate a new measurement value for this model grid. With this approach, one new measurement thus almost corresponds to one model state point, which means the representation error of the model is probably small. For the moment we will therefore not explicitly specify a model representation error, but implicitly assume that it is zero. Therefore, the total measurement error used in data assimilation, is equal to the extraction error in this study.

After the measurements of concentrations are extracted and the total measurement error is quantified, EnSR can be used to combine them with the LOTOS-EUROS model running to reconstruct optimal estimates.

4.3 Assimilation performance

In the following, we first examine how data assimilation actually works in the system (see Fig. 4). The first assimilation result with EnSR (Fig. 4**a**, **b**), at 01:00 UTC 16 May 2010, is shown against the SEVIRI extracted measurements (Fig. 4**c**). Ensemble-

based data assimilation includes two steps (forecast and analysis, see Appendix A). After one-day of model running started from 00:00 UTC 15 May 2010, the EnSR forecasted state at 01:00 UTC 16 May 2010 is shown in Fig. 4**a**. Comparing the state to the extracted measurements (Fig. 4**c**), the former (with concentrations higher than 2.0 mg m^{-3} in the main plume) shows a much larger estimation compared to the latter (with concentrations mostly lower than 0.8 mg m^{-3}). After the EnSR analysis step (see Fig. 4**b**), the concentrations in large parts are now closer to the extracted measurements. In reality, a potential overestimation is usually elusive and hard to avoid, which is mainly due to lack of sedimentation processes (Fu et al., 2016). The comparison between the state of analysis and forecast illustrates that the EnSR assimilation process can potentially solve the problem of overestimation. Note that, in this study only PM_{10} ash component is considered in the assimilation system, which is consistent with that during satellite retrievals, only the fine particles (mostly with sizes <10.0 μm) can be detected in the tropospheric volcanic plume based on the robust and reliable retrieval algorithms (Prata, 1989; Corradini et al., 2008). It is also the main mass fraction that is transported at large distances from the source, since most of the large particles (and therefore mass) is removed quickly from the plume.

The results above were compared in terms of concentrations, not the original mass loadings. To guarantee the assimilation performance, the comparison in concentrations only is not sufficient, because the original data is not concentrations but mass loadings. If SOO is not accurate enough for extracting the concentrations at specified heights, the assimilation results still can approximate well the inaccurate extracted concentrations due to the intrinsic forcing of ensemble-based algorithms. Obviously, the approximation in this case is incorrect. Based on this consideration, original measurements (i.e., SEVIRI ash mass loadings, see Fig. 5**a**) need to be employed for a further validation. After two-days continuously assimilating SEVIRI measurements of the extracted PM_{10} concentrations, the analyzed volcanic ash state at 00:00 UTC 18 May 2010 is shown in in Fig. 5**c**. The conventional simulation without assimilation is also presented (Fig. 5**b**), which is currently the commonly used strategy for the simulation of volcanic ash transport (Webley et al., 2012; Fu et al., 2015). It is clear that the mass loadings with EnSR are in a good agreement with the SEVIRI mass loadings, in almost the entire plume. For example, in the area of the Netherlands, the mass loadings from EnSR are accumulated to 2.9 – 3.2 g m^{-2}, which is in good match with SEVIRI retrieved 3.1 g m^{-2}. While with the conventional simulation, the mass loadings in this area exceed 5.0 g m^{-2}. It can be seen that EnSR effectively decreases the estimation level compared to the conventional simulation. Because the measurements used in the assimilation system are extracted with the SOO, thus the good results with respect to mass loadings also verify the suitability of SOO for extracting reliable 3D concentrations. Note that here we also checked the SEVIRI mass loading retrieval error and the standard deviation of the mass loadings, and found that both have the same order of magnitude.

5 Quantification of the effective forecast duration using aircraft in situ measurements

According to discussions above, the accuracy of volcanic ash state is significantly improved by ensemble-based data assimilation after a continuous assimilation period (e.g., two days). Apparently, with the improved state as initialization, an improved forecast can be obtained (Fu et al., 2015). However, it remains unknown how long the improvement on forecasts will last.

To investigate the effective duration of the improved ash forecasts after assimilation, a one-day forecast is performed by initializing EnSR analyzed state (Fig. 5**b**) at 00:00 UTC 18 May 2010. For this investigation, the best way is to compare the forecasted concentrations with high-accurate real-time measurements. Satellite-based data may not be the best choice because usually there are big uncertainties in the measurements (Prata and Prata, 2012; Lu et al., 2016b). Aircraft-based measurements can be the optimal type of observations for this investigation, because the measurements allow sampling of the ash cloud with a high spatial and temporal resolution and by using optical particle counters (OPC) this type of measurement is estimated at a high accuracy of 10% (Weber et al., 2010).

Fortunately, some aircraft measurements on 18 May 2010 from 09:30 to 15:30 UTC are available, which were performed by the group Environmental Measurement Techniques at Düsseldorf university of Applied Sciences. The measurements took place in the North-West part of Germany including the border between the Netherlands and Germany, see Fig. 6**a**. The aircraft took off from the airfield "Schwarze Heide" in the Northern part of the Rhein-Ruhr area, headed along the Dutch-German border in the direction of the North Sea, continued towards Hamburg and then returned to the airfield. Along the route, concentrations of PM_{10} and $PM_{2.5}$ were measured. Fig. 6**b** and 6**c** are the comparison of aircraft PM_{10} measurements against the forecasted concentrations after assimilation and without assimilation.

For the period from 09:30 to 11:00 UTC (Fig. 6**b**), although the forecasting time has been over 9 hours (i.e., the last assimilation is 9 hours ago), the forecasted concentrations still have a good match with the accurate aircraft measurements, while the conventional forecast (i.e., forecast without assimilation) doesn't. This result shows the forecast over 11 hours after assimilation has also a high accuracy compared to the measurements. The result can be extended to 15 hours comparing with the other period from 12:30 to 15:00 UTC (Fig. 6**c**). Therefore, the validation test with aircraft in situ measurements shows that the regional forecasts (i.e., in the regions of North-West part of Germany) after satellite data assimilation remains valid and accurate for at least 15 hours. This is an important indication about how long a valid regional aviation advice based on the forecast after assimilation can last. This time duration lasts probably even longer, but we don't have aircraft measurements later than 15 hours available to evaluate this. Considering that this duration is likely to be dependent on the weather dynamics, so in this study we quantify the effective time duration at a shorter length for a conservative estimate, e.g., 12 hours (a half day).

6 Conclusions

In this paper, we choose the Eyjafjallajökull volcanic ash plume in May 2010 as the study case. In this study, a satellite observational operator (SOO) was developed to translate 2D satellite ash mass loadings to 3D ash concentrations at the top layer of volcanic ash clouds. To extract ash concentrations, not only the SEVIRI data of ash mass loadings, ash cloud top height are employed, but also a reasonable assumption of the ash cloud thickness range (0.5–3 km), at the corresponding horizontal location of the SEVIRI retrieved measurements, are combined. The advantage of SOO is that it can use rough thickness information to get uncertain concentrations, which are suitable for the data assimilation methodology.

The extracted ash concentration measurements enable us to perform ensemble-based data assimilation in a 3D volcanic ash transport model. By employing a preprocessing procedure before data assimilation to generate new measurement values by averaging all surrounding measurements, the model representation error is approximately zero. The extraction error is also calculated, and the total measurement error (defined as the sum of the extraction error and the model representation error) is therefore quantified, which together with the concentrations describe the 3D measurements (mean, error) for a data assimilation system. The results showed the assimilation significantly reduces the estimation level of the conventional simulation. The accuracy of the volcanic ash state was shown to be significantly improved by the assimilation of satellite mass loadings. The good assimilation performance also verifies the suitability of the proposed SOO.

With the improved volcanic ash state as initialization, improved volcanic ash forecasts are obtained. Quantification using highly accurate aircraft in situ measurements showed that the regional forecasts after satellite data assimilation remain valid and accurate up to a half day. This effective time period probably lasts even longer and this should be further tested when more aircraft measurements are available.

In this study, we developed SOO by considering cases where one singular ash cloud is present. Actually, it could happen that there are several isolated volcanic ash clouds in the vertical direction. The methodology of SOO is also valid for these cases, where the top isolated ash cloud does not correspond to the full but to a fraction of SEVERI ash mass loadings. How to determine the reasonable proportions/percentages for multiple isolated vertical ash clouds will be investigated in future.

In this paper, we applied an off-line approach for model running and simply used the deterministic meteorological input data. Actually these data also contain uncertainties which have an influence on ash cloud transport. In future work, for more accurate ash forecasting, uncertainties in the meteorological data like wind speed should also be taken into account.

7 Data availability

All the satellite data shown in Fig. 1 are available and can be downloaded from http://vast.nilu.no/test-database/volcano/Eyjafjallajokull/eruption/2010-04-14/main_data_type/Satellite/specific_data_type/seviri/ (Registration required). The averaged aircraft in situ data used in this study are available from Fig. 6**b**, **c**. The used continuous aircraft data and the model output data can be accessed by request (G.Fu@tudelft.nl).

Appendix A: The ensemble square root filter

The ensemble square root filter (EnSR) is essentially a Monte Carlo sequential method (Evensen, 2003), based on the representation of the probability density of the state estimate by an ensemble of N states, $\xi_1, \xi_2, \cdots, \xi_N$. Each ensemble member is assumed as one sample of a true state distribution. The required ensemble size depends on the model's nonlinearity and the the involved uncertainties. For the application of the filter algorithm to a volcanic ash transport model, an ensemble size of 50 is considered acceptable for maintaining a balance between accuracy and computational cost (Fu et al., 2015, 2016). In the first step of this algorithm an ensemble of N volcanic ash state $\xi^a(0)$ is generated to represent the uncertainty in the initial

condition $\mathbf{x}(0)$. In the second step (the forecast step), the model propagates the ensemble members from time t_{k-1} to t_k:

$$\xi_j^f(k) = M_{k-1}(\xi_j^a(k-1)). \tag{A1}$$

The state-space operator M_{k-1} describes the time evolution from the time t_{k-1} to t_k of the state vector which contains the ash concentrations in all the model grid boxes. The filter state at time t_k is a stochastic distribution with mean $\mathbf{x}^f$ and covariance $\mathbf{P}^f$ given by:

$$\mathbf{x}^f = \frac{1}{N}[\sum_{j=1}^{N} \xi_j^f] \quad , \tag{A2}$$

$$\mathbf{L}^f = [\xi_1^f - \mathbf{x}^f, \cdots, \xi_N^f - \mathbf{x}^f] \quad , \tag{A3}$$

$$\mathbf{P}^f = \frac{1}{N-1}[\mathbf{L}^f(\mathbf{L}^f)'] \quad , \tag{A4}$$

The observational network at time t_k is defined by the observation operator H that maps state vector $\mathbf{x}$ to observation space $\mathbf{y}$ by $\mathbf{y}(k) = H_k(\mathbf{x}(k)) + \mathbf{v}(k)$, where the observation error $\mathbf{v}$ is drawn from Gaussian distribution with zero mean and covariance matrix $\mathbf{R}$. Here, $\mathbf{y}$ contains the measurements of ash concentrations and $\mathbf{R}$ is assumed to be a diagonal matrix with the square of the standard deviation (measurement uncertainty) as diagonal entries. The operator H selects the grid cell in $\mathbf{x}(k)$ that corresponds to the observation location. When measurements become available, the ensemble members are updated in the analysis step using the Kalman gain and their ensemble covariance matrix following:

$$\mathbf{K} = \mathbf{P}^f\mathbf{H}'[\mathbf{H}\mathbf{P}^f\mathbf{H}' + \mathbf{R}]^{-1} \quad , \tag{A5}$$

$$\xi_j^a = \xi_j^f + \mathbf{K}[\mathbf{y} - \mathbf{H}\xi_j^f + \mathbf{v}_j] \quad , \tag{A6}$$

$$\mathbf{P}^a = (\mathbf{I} - \mathbf{K}\mathbf{H})\mathbf{P}^f \quad , \tag{A7}$$

where $\mathbf{v}_j$ represents realizations of the observation error v. To reduce the sampling errors introduced by adding random numbers $\mathbf{v}_j$ to the observations, the analysis step can be written in a square root form (Evensen, 2004; Sakov and Oke, 2008a, b). Using the notations $\mathbf{Y} = \mathbf{H}\mathbf{L}^f$ and $\mathbf{S} = \mathbf{Y}\mathbf{Y}' + \mathbf{R}$, the updated covariance matrix becomes:

$$\mathbf{P}^a = \mathbf{L}^a(\mathbf{L}^a)' = \mathbf{L}^f(\mathbf{I} - \mathbf{Y}'\mathbf{S}^{-1}\mathbf{Y})(\mathbf{L}^f)' = \mathbf{L}^f\mathbf{T}\mathbf{T}'(\mathbf{L}^f)' \quad , \tag{A8}$$

thus $\mathbf{L}^a$ can be represented by

$$\mathbf{L}^a = \mathbf{L}^f\mathbf{T} \quad , \tag{A9}$$

where $\mathbf{T}$ is an $N \times N$ matrix which satisfies: $\mathbf{T}\mathbf{T}' = \mathbf{I} - \mathbf{Y}'\mathbf{S}^{-1}\mathbf{Y}$. It can be easily shown that there is a unique symmetric positive definite solution defined as the square root of the symmetric positive definite matrix: $\mathbf{T}^s = [\mathbf{I} - \mathbf{Y}'\mathbf{S}^{-1}\mathbf{Y}]^{\frac{1}{2}}$. By using the eigenvalue decomposition, the matrix $\mathbf{T}^s$ has the following form:

$$\mathbf{T}^s = \mathbf{C}\mathbf{\Lambda}^{\frac{1}{2}}\mathbf{C}', \tag{A10}$$

where $\mathbf{T}^s$ is referred as the symmetric factor. The symmetric algorithm defined above introduces the smallest analysis increments for an arbitrary compatible norm. The good performance of EnSR has been obtained on improving the forecast accuracies without introducing additional sampling errors (Evensen, 2004; Sakov and Oke, 2008a).

Author contributions. All authors participated in the design of the experiment and the analysis of the assimilation results. Guangliang Fu, Arjo Segers and Sha Lu modeled the volcanic ash transport using the LOTOS-EUROS. Fred Prata and Guangliang Fu validated SEVIRI measurements and provided them for the development of SSO. Guangliang Fu, Hai Xiang Lin and Arnold Heemink carried out data assimilation experiment, analyzed the results and finalized the paper.

Acknowledgements. We are very grateful to the editor and reviewers for their reviews and insightful comments. We thank European Space Agency (ESA) project – Volcanic Ash Strategic initiative Team (VAST) for providing the satellite data for the 2010 Eyjafjallajökull volcanic eruption. We thank Prof. Konradin Weber (University of Applied Sciences, Environmental Measurement Techniques, Düsseldorf, Germany) for providing the real-time aircraft in situ measurements. We thank Dr. Arve Kylling (Senior scientist in NILU-Norwegian Institute for Air Research) for his kind assistance with interpretations of available satellite data. In this paper, we perform the ensemble-based data assimilation using OpenDA (open source software, www.openda.com). The first and the last author thank the research funds by China Scholarship Council. We would also like to thank the Netherlands Supercomputing Centre (SURFsara) for providing us the computing facility: the Cartesius cluster.

References

Ansmann, A., Tesche, M., Groß, S., Freudenthaler, V., Seifert, P., Hiebsch, A., Schmidt, J., Wandinger, U., Mattis, I., Müller, D., and Wiegner, M.: The 16 April 2010 major volcanic ash plume over central Europe: EARLINET lidar and AERONET photometer observations at Leipzig and Munich, Germany, Geophys. Res. Lett., 37, L13 810+, doi:10.1029/2010gl043809, 2010.

Bocquet, M., Elbern, H., Eskes, H., Hirtl, M., Žabkar, R., Carmichael, G. R., Flemming, J., Inness, A., Pagowski, M., Pérez Camaño, J. L., Saide, P. E., San Jose, R., Sofiev, M., Vira, J., Baklanov, A., Carnevale, C., Grell, G., and Seigneur, C.: Data assimilation in atmospheric chemistry models: current status and future prospects for coupled chemistry meteorology models, Atmospheric Chemistry and Physics, 15, 5325–5358, doi:10.5194/acp-15-5325-2015, 2015.

Bonadonna, C. and Costa, A.: Plume height, volume, and classification of explosive volcanic eruptions based on the Weibull function, 75, 1–19, doi:10.1007/s00445-013-0742-1, 2013.

Casadevall, T. J.: The 1989–1990 eruption of Redoubt Volcano, Alaska: impacts on aircraft operations, Journal of Volcanology and Geothermal Research, 62, 301–316, doi:10.1016/0377-0273(94)90038-8, 1994.

Clarisse, L. and Prata, F.: Infrared Sounding of Volcanic Ash, pp. 189–215, Elsevier, doi:10.1016/b978-0-08-100405-0.00017-3, 2016.

Corradini, S., Spinetti, C., Carboni, E., Tirelli, C., Buongiorno, M. F., Pugnahi, S., and Gangale, G.: Mt. Etna tropospheric ash retrieval and sensitivity analysis using moderate resolution imaging spectroradiometer measurements, Journal of Applied Remote Sensing, 2, 023 550–023 550–20, doi:10.1117/1.3046674, 2008.

Dacre, H. F., Grant, A. L. M., Harvey, N. J., Thomson, D. J., Webster, H. N., and Marenco, F.: Volcanic ash layer depth: Processes and mechanisms, Geophys. Res. Lett., 42, 2014GL062 454+, doi:10.1002/2014gl062454, 2015.

de Laat, A. T. J. and van der A, R. J.: Validation and evaluation of SEVIRIvolcanic ash heights, Tech. rep., Royal Netherlands Meteorological Institute (KNMI), http://bibliotheek.knmi.nl/knmipubTR/TR337.pdf, 2012.

Draxler, R. R. and Hess, G. D.: An overview of the HYSPLIT_4 modelling system for trajectories, dispersion, and deposition, Australian Meteorological Magazine, 47, 295–308, http://www.arl.noaa.gov/documents/reports/MetMag.pdf, 1998.

EASA: EASA Safety Information Bulletin 2010-17R7, http://ad.easa.europa.eu/ad/2010-17R7, 2015.

Eliasson, J., Palsson, A., and Weber, K.: Monitoring ash clouds for aviation, Nature, 475, 455, doi:10.1038/475455b, 2011.

Emeis, S., Forkel, R., Junkermann, W., Schäfer, K., Flentje, H., Gilge, S., Fricke, W., Wiegner, M., Freudenthaler, V., Groβ, S., Ries, L., Meinhardt, F., Birmili, W., Münkel, C., Obleitner, F., and Suppan, P.: Measurement and simulation of the 16/17 April 2010 Eyjafjallajökull volcanic ash layer dispersion in the northern Alpine region, Atmospheric Chemistry and Physics, 11, 2689–2701, doi:10.5194/acp-11-2689-2011, 2011.

Evensen, G.: Sequential data assimilation with a nonlinear quasi-geostrophic model using Monte Carlo methods to forecast error statistics, J. Geophys. Res., 99, 10 143–10 162, doi:10.1029/94jc00572, 1994.

Evensen, G.: The Ensemble Kalman Filter: theoretical formulation and practical implementation, Ocean Dynamics, 53, 343–367, doi:10.1007/s10236-003-0036-9, 2003.

Evensen, G.: Sampling strategies and square root analysis schemes for the EnKF, Ocean Dynamics, 54, 539–560, doi:10.1007/s10236-004-0099-2, 2004.

Evensen, G. and van Leeuwen, P. J.: An Ensemble Kalman Smoother for Nonlinear Dynamics, Mon. Wea. Rev., 128, 1852–1867, doi:10.1175/1520-0493(2000)128%3C1852:aeksfn%3E2.0.co;2, 2000.

Flentje, H., Claude, H., Elste, T., Gilge, S., Köhler, U., Plass-Dülmer, C., Steinbrecht, W., Thomas, W., Werner, A., and Fricke, W.: The Eyjafjallajökull eruption in April 2010 – detection of volcanic plume using in-situ measurements, ozone sondes and a new generation ceilometer network, Atmospheric Chemistry and Physics Discussions, 10, 14 947–14 968, doi:10.5194/acpd-10-14947-2010, 2010.

Francis, P. N., Cooke, M. C., and Saunders, R. W.: Retrieval of physical properties of volcanic ash using Meteosat: A case study from the 2010 Eyjafjallajökull eruption, J. Geophys. Res., 117, D00U09+, doi:10.1029/2011jd016788, 2012.

Fu, G., Lin, H. X., Heemink, A. W., Segers, A. J., Lu, S., and Palsson, T.: Assimilating aircraft-based measurements to improve Forecast Accuracy of Volcanic Ash Transport, Atmospheric Environment, 115, 170–184, doi:10.1016/j.atmosenv.2015.05.061, 2015.

Fu, G., Heemink, A., Lu, S., Segers, A., Weber, K., and Lin, H.-X.: Model-based aviation advice on distal volcanic ash clouds by assimilating aircraft in situ measurements, Atmospheric Chemistry and Physics, 16, 9189–9200, doi:10.5194/acp-16-9189-2016, 2016.

Gieske, A. S. M., Hendrikse, J., Retsios, V., van Leeuwen, B., Maathuis, B. H. P., Romaguera, M., Sobrino, J. A., Timmermans1, W. J., and Su1, Z.: Processing of MSG-1 SEVIRI data in the thermal infrared–Algorithm development with the use of the SPARC 2004 data set, in: Proc. WPP-250: SPARC Final Workshop, pp. 1–8, Enschede, Netherlands, http://www.itc.nl/library/papers_2005/conf/gieske_pro.pdf, 2005.

Jones, A., Thomson, D., Hort, M., and Devenish, B.: The U.K. Met Office's Next-Generation Atmospheric Dispersion Model, NAME III, in: Air Pollution Modeling and Its Application XVII, edited by Borrego, C. and Norman, A.-L., pp. 580–589, Springer US, doi:10.1007/978-0-387-68854-1_62, 2007.

Kylling, A., Kristiansen, N., Stohl, A., Buras-Schnell, R., Emde, C., and Gasteiger, J.: A model sensitivity study of the impact of clouds on satellite detection and retrieval of volcanic ash, Atmospheric Measurement Techniques, 8, 1935–1949, doi:10.5194/amt-8-1935-2015, 2015.

Lu, S., Lin, H. X., Heemink, A., Segers, A., and Fu, G.: Estimation of volcanic ash emissions through assimilating satellite data and ground-based observations, J. Geophys. Res. Atmos., 121, 1–24, doi:10.1002/2016JD025131, 2016a.

Lu, S., Lin, H. X., Heemink, A. W., Fu, G., and Segers, A. J.: Estimation of Volcanic Ash Emissions Using Trajectory-Based 4D-Var Data Assimilation, Mon. Wea. Rev., 144, 575–589, doi:10.1175/mwr-d-15-0194.1, 2016b.

Marenco, F., Johnson, B., Turnbull, K., Newman, S., Haywood, J., Webster, H., and Ricketts, H.: Airborne lidar observations of the 2010 Eyjafjallajökull volcanic ash plume, J. Geophys. Res., 116, D00U05+, doi:10.1029/2011jd016396, 2011.

Mastin, L. G., Guffanti, M., Servranckx, R., Webley, P., Barsotti, S., Dean, K., Durant, A., Ewert, J. W., Neri, A., Rose, W. I., Schneider, D., Siebert, L., Stunder, B., Swanson, G., Tupper, A., Volentik, A., and Waythomas, C. F.: A multidisciplinary effort to assign realistic source parameters to models of volcanic ash-cloud transport and dispersion during eruptions, Journal of Volcanology and Geothermal Research, 186, 10–21, doi:10.1016/j.jvolgeores.2009.01.008, 2009.

Oberhuber, J. M., Herzog, M., Graf, H.-F., and Schwanke, K.: Volcanic plume simulation on large scales, Journal of Volcanology and Geothermal Research, 87, 29–53, doi:10.1016/s0377-0273(98)00099-7, 1998.

Oxford-Economics: The Economic Impacts of Air Travel Restrictions Due to Volcanic Ash, Report for Airbus, Tech. rep., http://www.oxfordeconomics.com/my-oxford/projects/129051, 2010.

Pappalardo, G., Amodeo, A., Ansmann, A., Apituley, A., Alados Arboledas, L., Balis, D., Böckmann, C., Chaikovsky, A., Comeron, A., D'Amico, G., De Tomasi, F., Freudenthaler, V., Giannakaki, E., Giunta, A., Grigorov, I., Gustafsson, O., Gross, S., Haeffelin, M., Iarlori, M., Kinne, S., Linné, H., Madonna, F., Mamouri, R., Mattis, I., McAuliffe, M., Molero, F., Mona, L., Müller, D., Mitev, V., Nicolae, D., Papayannis, A., Perrone, M. R., Pietruczuk, A., Pujadas, M., Putaud, J.-P., Ravetta, F., Rizi, V., Serikov, I., Sicard, M., Simeonov, V.,

Spinelli, N., Stebel, K., Trickl, T., Wandinger, U., Wang, X., Wagner, F., and Wiegner, M.: EARLINET observations of the Eyjafjallajökull ash plume over Europe, vol. 7832, pp. 78 320J–78 320J–9, doi:10.1117/12.869016, 2010.

Pavolonis, M. J.: Advances in Extracting Cloud Composition Information from Spaceborne Infrared Radiances—A Robust Alternative to Brightness Temperatures. Part I: Theory, J. Appl. Meteor. Climatol., 49, 1992–2012, doi:10.1175/2010jamc2433.1, 2010.

Prata, A. J.: Infrared radiative transfer calculations for volcanic ash clouds, Geophys. Res. Lett., 16, 1293–1296, doi:10.1029/gl016i011p01293, 1989.

Prata, A. J. and Prata, A. T.: Eyjafjallajökull volcanic ash concentrations determined using Spin Enhanced Visible and Infrared Imager measurements, Journal of Geophysical Research: Atmospheres, 117, n/a, doi:10.1029/2011jd016800, 2012.

Prata, A. T., Siems, S. T., and Manton, M. J.: Quantification of volcanic cloud top heights and thicknesses using A-train observations for the 2008 Chaitén eruption, J. Geophys. Res. Atmos., 120, 2014JD022 399+, doi:10.1002/2014jd022399, 2015.

Sakov, P. and Oke, P. R.: A deterministic formulation of the ensemble Kalman filter: an alternative to ensemble square root filters, Tellus A, 60, 361–371, doi:10.1111/j.1600-0870.2007.00299.x, 2008a.

Sakov, P. and Oke, P. R.: Implications of the Form of the Ensemble Transformation in the Ensemble Square Root Filters, Mon. Wea. Rev., 136, 1042–1053, doi:10.1175/2007mwr2021.1, 2008b.

Schaap, M., Timmermans, R. M. A., Roemer, M., Boersen, G. A. C., Builtjes, P. J. H., Sauter, F. J., Velders, G. J. M., and Beck, J. P.: The LOTOS EUROS model: description, validation and latest developments, International Journal of Environment and Pollution, 32, 270+, doi:10.1504/ijep.2008.017106, 2008.

Schäfer, K., Thomas, W., Peters, A., Ries, L., Obleitner, F., Schnelle-Kreis, J., Birmili, W., Diemer, J., Fricke, W., Junkermann, W., Pitz, M., Emeis, S., Forkel, R., Suppan, P., Flentje, H., Gilge, S., Wichmann, H. E., Meinhardt, F., Zimmermann, R., Weinhold, K., Soentgen, J., Münkel, C., Freuer, C., and Cyrys, J.: Influences of the 2010 Eyjafjallajökull volcanic plume on air quality in the northern Alpine region, Atmospheric Chemistry and Physics, 11, 8555–8575, doi:10.5194/acp-11-8555-2011, 2011.

Schmetz, J., Pili, P., Tjemkes, S., Just, D., Kerkmann, J., Rota, S., and Ratier, A.: An Introduction to Meteosat Second Generation (MSG), Bull. Amer. Meteor. Soc., 83, 977–992, doi:10.1175/1520-0477(2002)083%3C0977:aitmsg%3E2.3.co;2, 2002.

Schumann, U., Weinzierl, B., Reitebuch, O., Schlager, H., Minikin, A., Forster, C., Baumann, R., Sailer, T., Graf, K., Mannstein, H., Voigt, C., Rahm, S., Simmet, R., Scheibe, M., Lichtenstern, M., Stock, P., Rüba, H., Schäuble, D., Tafferner, A., Rautenhaus, M., Gerz, T., Ziereis, H., Krautstrunk, M., Mallaun, C., Gayet, J. F., Lieke, K., Kandler, K., Ebert, M., Weinbruch, S., Stohl, A., Gasteiger, J., Groß, S., Freudenthaler, V., Wiegner, M., Ansmann, A., Tesche, M., Olafsson, H., and Sturm, K.: Airborne observations of the Eyjafjalla volcano ash cloud over Europe during air space closure in April and May 2010, Atmospheric Chemistry and Physics, 11, 2245–2279, doi:10.5194/acp-11-2245-2011, 2011.

Searcy, C., Dean, K., and Stringer, W.: PUFF: A high-resolution volcanic ash tracking model, Journal of Volcanology and Geothermal Research, 80, 1–16, doi:10.1016/s0377-0273(97)00037-1, 1998.

Stohl, A., Prata, A. J., Eckhardt, S., Clarisse, L., Durant, A., Henne, S., Kristiansen, N. I., Minikin, A., Schumann, U., Seibert, P., Stebel, K., Thomas, H. E., Thorsteinsson, T., Tørseth, K., and Weinzierl, B.: Determination of time- and height-resolved volcanic ash emissions and their use for quantitative ash dispersion modeling: the 2010 Eyjafjallajökull eruption, Atmospheric Chemistry and Physics, 11, 4333–4351, doi:10.5194/acp-11-4333-2011, 2011.

Verlaan, M. and Heemink, A. W.: Tidal flow forecasting using reduced rank square root filters, Stochastic Hydrology and Hydraulics, 11, 349–368, doi:10.1007/bf02427924, 1997.

Weber, K., Vogel, A., Fischer, C., van Haren, G., and Pohl, T.: Airborne measurements of the Eyjafjallajökull volcanic ash plume over northwestern Germany with a light aircraft and an optical particle counter: first results, vol. 7832, pp. 78 320P–78 320P–15, doi:10.1117/12.869629, 2010.

Weber, K., Eliasson, J., Vogel, A., Fischer, C., Pohl, T., van Haren, G., Meier, M., Grobéty, B., and Dahmann, D.: Airborne in-situ investigations of the Eyjafjallajökull volcanic ash plume on Iceland and over north-western Germany with light aircrafts and optical particle counters, Atmospheric Environment, 48, 9–21, doi:10.1016/j.atmosenv.2011.10.030, 2012.

Webley, P. W., Steensen, T., Stuefer, M., Grell, G., Freitas, S., and Pavolonis, M.: Analyzing the Eyjafjallajökull 2010 eruption using satellite remote sensing, lidar and WRF-Chem dispersion and tracking model, J. Geophys. Res., 117, D00U26+, doi:10.1029/2011jd016817, 2012.

Wiegner, M., Gasteiger, J., Groß, S., Schnell, F., Freudenthaler, V., and Forkel, R.: Characterization of the Eyjafjallajökull ash-plume: Potential of lidar remote sensing, Physics and Chemistry of the Earth, Parts A/B/C, 45-46, 79–86, doi:10.1016/j.pce.2011.01.006, 2012.

Winker, D. M., Liu, Z., Omar, A., Tackett, J., and Fairlie, D.: CALIOP observations of the transport of ash from the Eyjafjallajökull volcano in April 2010, Journal of Geophysical Research: Atmospheres, 117, n/a, doi:10.1029/2011jd016499, 2012.

Witham, C. S., Hort, M. C., Potts, R., Servranckx, R., Husson, P., and Bonnardot, F.: Comparison of VAAC atmospheric dispersion models using the 1 November 2004 Grimsvötn eruption, Met. Apps, 14, 27–38, doi:10.1002/met.3, 2007.

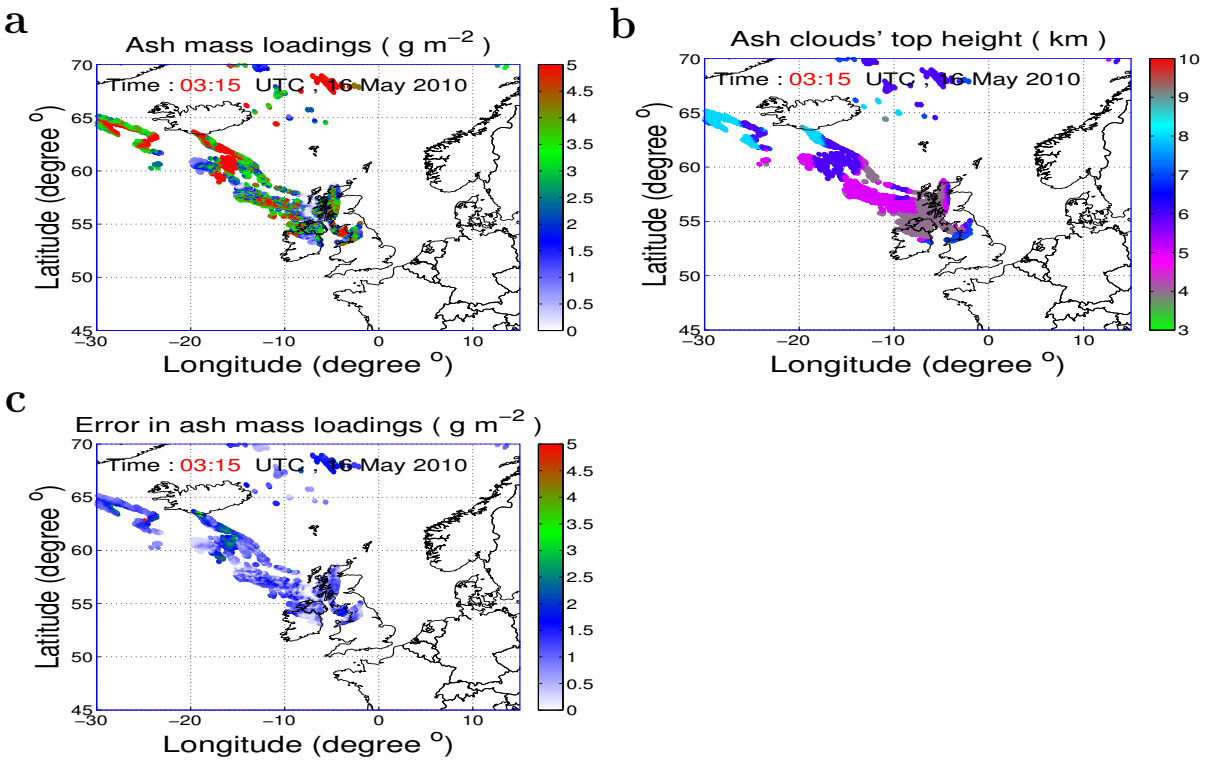

Figure 1. Available volcanic ash data from SEVIRI on 16 May 2010 at 03:15 UTC. Data are acquired from the European Space Agency (ESA) funded projects Volcanic Ash Strategic Initiative Team (VAST). **a**, Ash mass loadings. Values at 0 mean no data. **b**, Ash cloud top height. **c**, Error in the retrieved ash mass loadings.

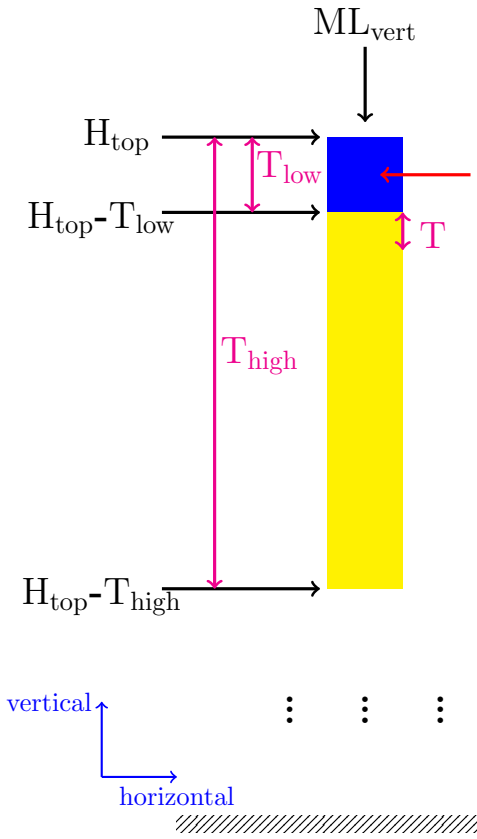

Notations

ML_{vert}	mass loadings in vertical direction
H_{top}	top height of ash clouds
T_{low}	lower bound of thickness (0.5 km)
T_{high}	upper bound of thickness (3.0 km)
T	a chosen thickness step length (0.05 km)

Figure 2. Illustration of the satellite observational operator (SOO). The ash concentration is extracted at the cloud top layer.

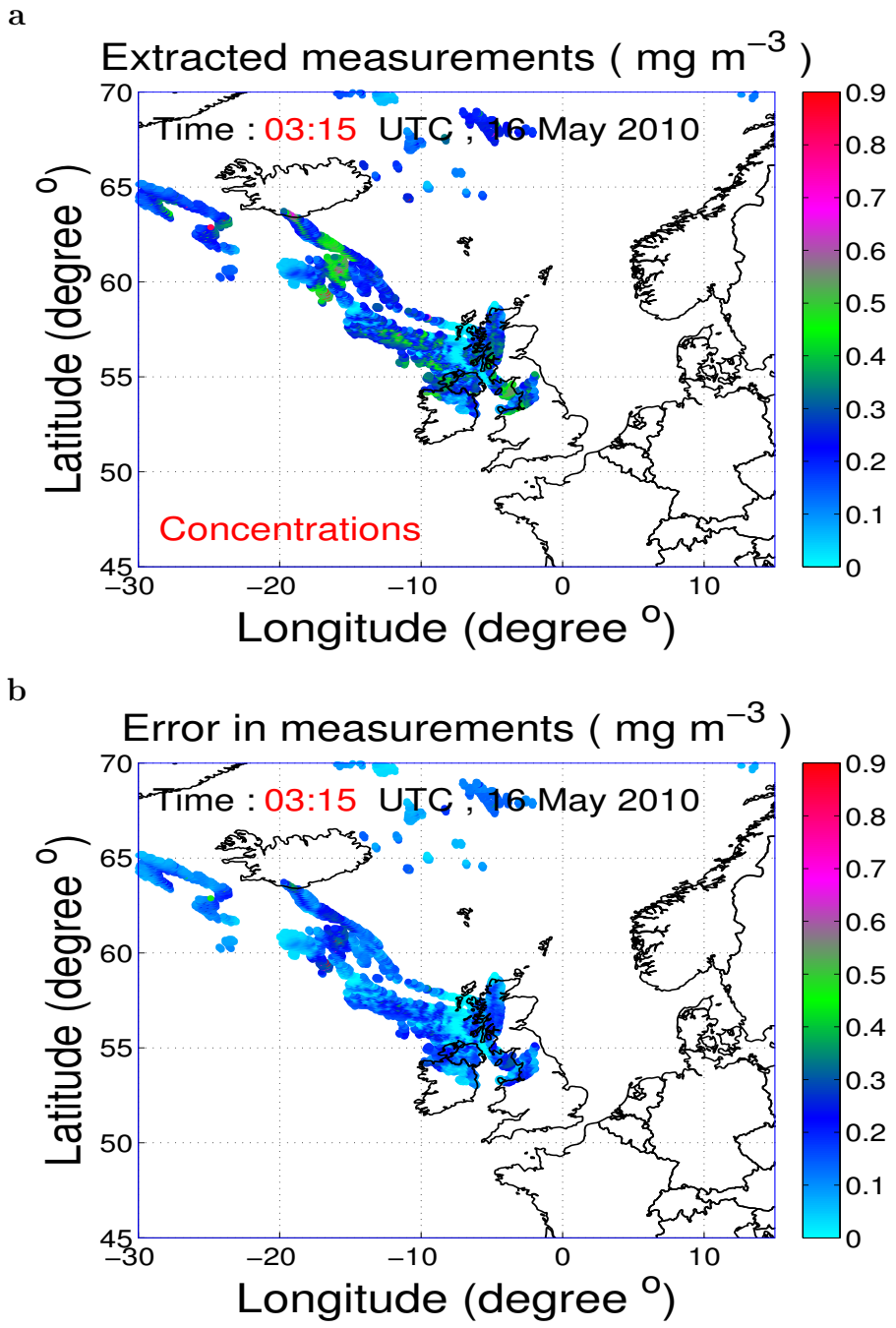

Figure 3. Results of the satellite observational operator (at 16 May 2010 at 03:15 UTC). a, Extracted ash concentrations at the cloud top layer. **b**, Error in the extracted ash concentrations.

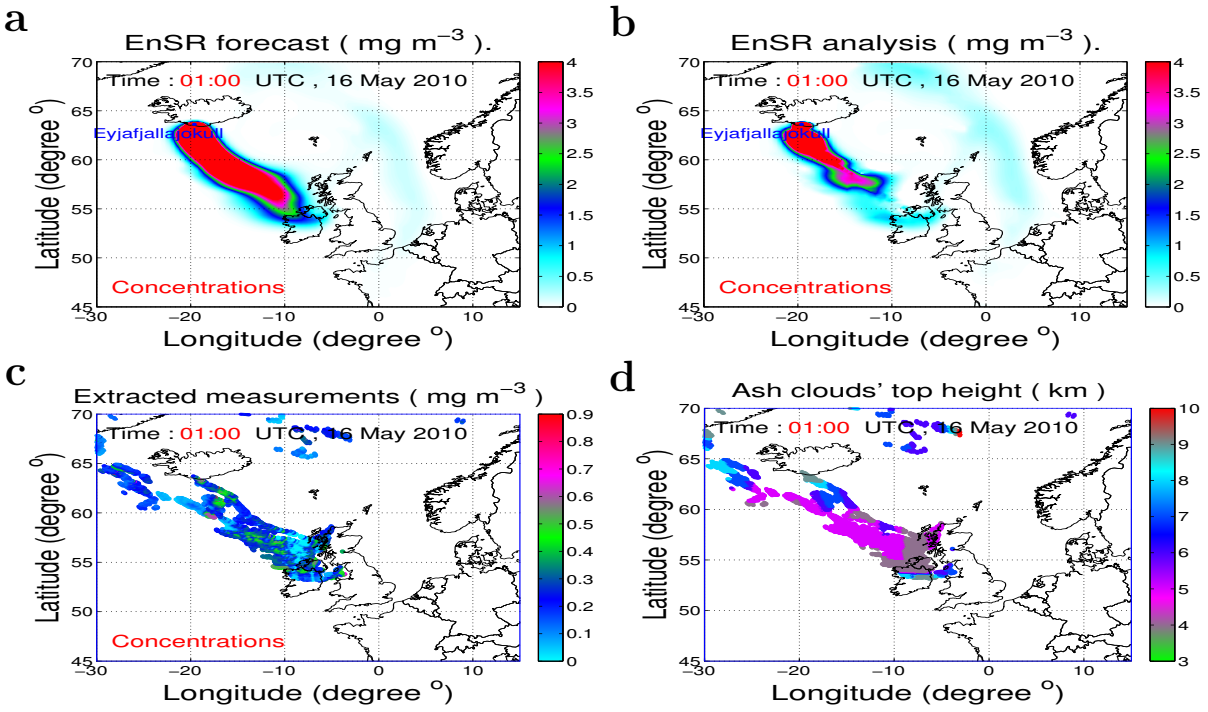

Figure 4. Examination of EnSR effect when assimilating SEVIRI-extracted ash concentrations at 01:00 UTC 16 May 2010. a, EnSR forecast (ensemble mean) of PM_{10} concentrations. **b**, EnSR analysis (ensemble mean) of PM_{10} concentrations. **c**, Extracted measurements of PM_{10} concentrations from the satellite observational operator. Ash concentrations shown in **a**, **b**, **c** are at the ash cloud top layer height **d**.

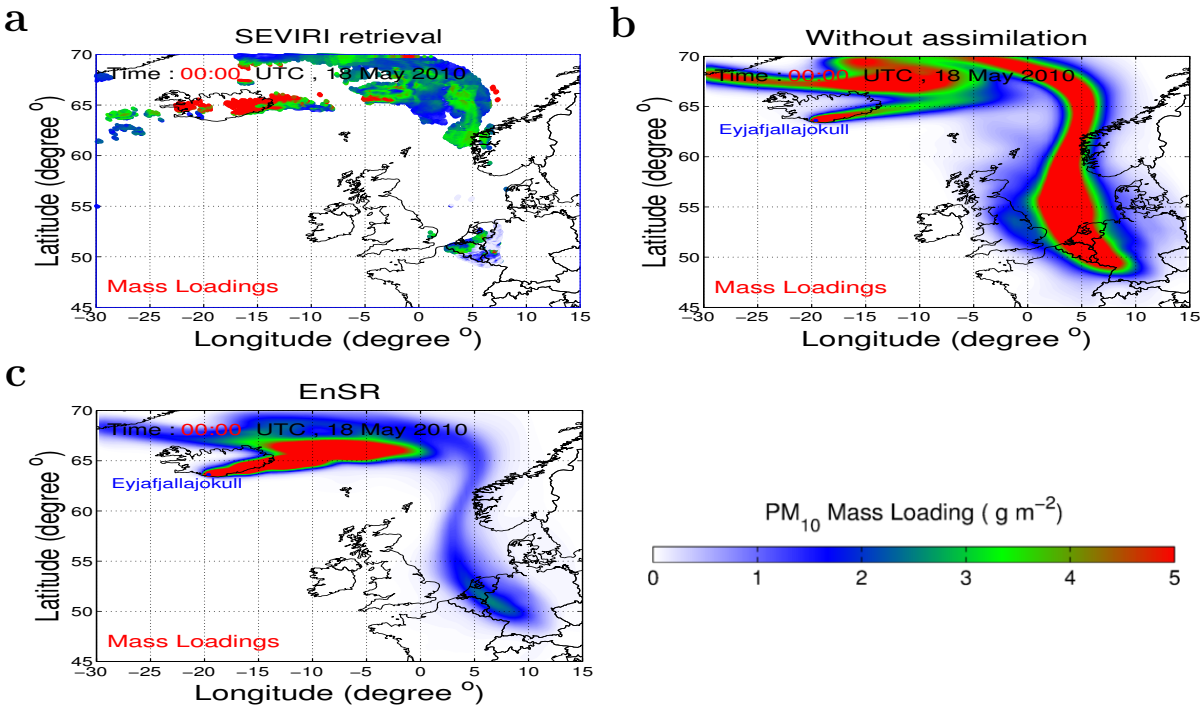

Figure 5. PM_{10} mass loadings with EnSR against the SEVIRI retrieval at 00:00 UTC 18 May 2010. a, SEVIRI retrieved mass loadings. **b**, Simulated mass loadings without assimilation. **c**, Mass loadings (ensemble mean) after 2-days EnSR assimilation.

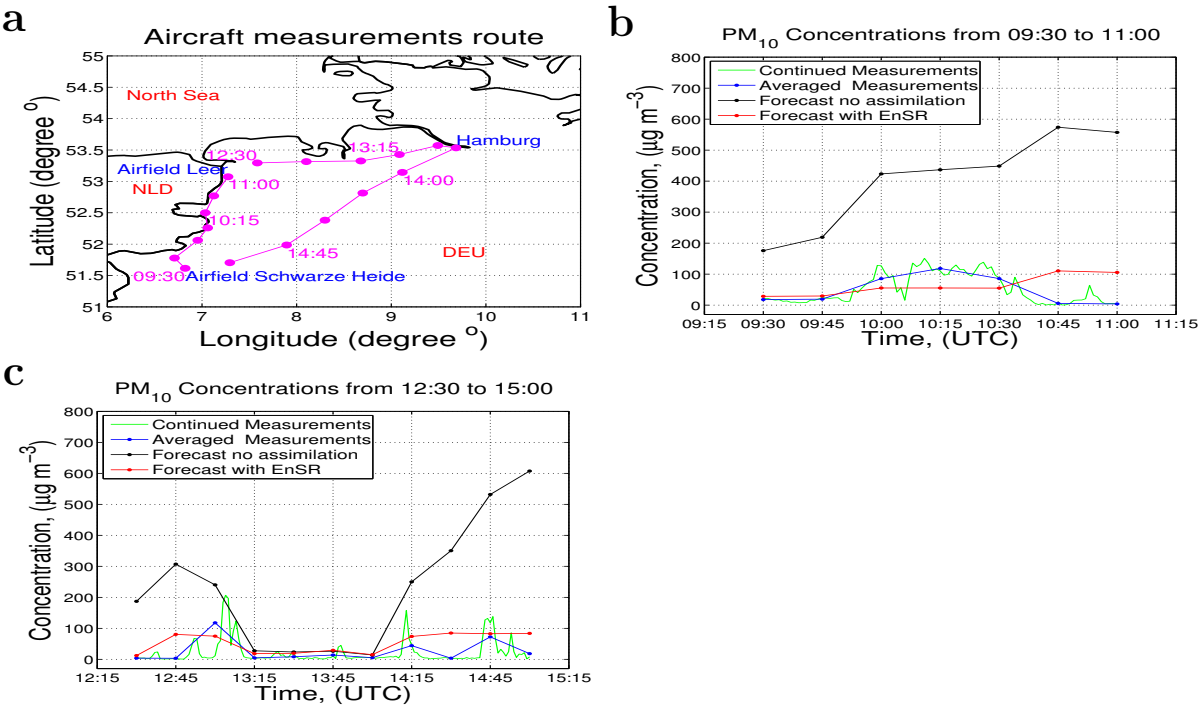

Figure 6. Quantification of effective assimilation forecasts using aircraft measurements (Date: 18 May 2010). a, Aircraft measurements route. **b**, Comparisons of measurements, forecasts after assimilation (ensemble mean) or without assimilation from 09:30 to 11:00 UTC. **c**, Comparisons from 12:30 to 15:00 UTC.